SURE 静岡大学学術リポジトリ
Shizuoka University REpository

Cavitand-Based Pd-Pyridyl Coordination Capsules: Guest-Induced Homo- or Heterocapsule Selection and Applications of Homocapsules to the Protection of a Photosensitive Guest and Chiral Capsule Formation

メタデータ	言語: English 出版者: 公開日: 2020-07-31 キーワード (Ja): キーワード (En): cage compounds, cavitands, host-guest systems, self-assembly, supramolecular chemistry 作成者: Nakamura, Munechika, Tsukamoto, Yoshimi, Ueta, Takuro, Sei, Yoshihisa, Fukushima, Takanori, Yoza, Kenji, Kobayashi, Kenji メールアドレス: 所属:
URL	http://hdl.handle.net/10297/00027568

Cavitand-Based Pd-Pyridyl Coordination Capsules: Guest-Induced Homo- or Heterocapsule Selection and Applications of Homocapsule to Protection of Photosensitive Guest and Chiral Capsule Formation

Munechika Nakamura,[a] Yoshimi Tsukamoto,[a] Takuro Ueta,[a] Yoshihisa Sei,[b] Takanori Fukushima,[b] Kenji Yoza,[c] and Kenji Kobayashi*[a,d]

[a] M. Nakamura, Y. Tsukamoto, T. Ueta, Prof. Dr. K. Kobayashi
Department of Chemistry, Faculty of Science
Shizuoka University
836 Ohya, Suruga-ku, Shizuoka 422-8529 (Japan)
E-mail: kobayashi.kenji.a@shizuoka.ac.jp

[b] Dr. Y. Sei, Prof. Dr. T. Fukushima
Laboratory for Chemistry and Life Science, Institute of Innovative Research
Tokyo Institute of Technology
4259 Nagatsuta, Midori-ku, Yokohama 226-8503 (Japan)

[c] Dr. K. Yoza
Bruker axs
3-9-B Moriya, Kanagawa-ku, Yokohama 221-0022 (Japan)

[d] Prof. Dr. K. Kobayashi
Research Institute of Green Science and Technology
Shizuoka University
836 Ohya, Suruga-ku, Shizuoka 422-8529 (Japan)

Supporting information for this article is given via a link at the end of the document.

Abstract: A 2:4 mixture of tetrakis[4-(4-pyridyl)phenyl]cavitand (**1**) or tetrakis[4-(4-pyridyl)phenylethynyl]cavitand (**2**) and Pd(dppp)$(OTf)_2$ self-assembles into a homocapsule $\{\mathbf{1}_2\cdot[Pd(dppp)]_4\}^{8+}\cdot(TfO^-)_8$ (**C1**) or $\{\mathbf{2}_2\cdot[Pd(dppp)]_4\}^{8+}\cdot(TfO^-)_8$ (**C2**), respectively, through Pd–Npy coordination bonds. A 1:1:4 mixture of **1**, **2**, and Pd(dppp)$(OTf)_2$ produced a mixture of homocapsules **C1**, **C2**, and a heterocapsule $\{\mathbf{1}\cdot\mathbf{2}\cdot[Pd(dppp)]_4\}^{8+}\cdot(TfO^-)_8$ (**C3**) in a 1:1:0.98 mole ratio. Selective formation (self-sorting) of homocapsules **C1** and **C2** or heterocapsule **C3** was controlled by guest-induced encapsulation under thermodynamic control. Applications of Pd–Npy coordination capsules with the use of **1** were demonstrated. Capsule **C1** serves as a guard nanocontainer for *trans*-4,4′-diacetoxyazobenzene to protect against the *trans*-to-*cis* photoisomerization by encapsulation. A chiral capsule $\{\mathbf{1}_2\cdot[Pd((R)\text{-BINAP})]_4\}^{8+}\cdot(TfO^-)_8$ (**C5**) was also constructed. Capsule **C5** induces supramolecular chirality with respect to prochiral 2,2′-bis(alkoxycarbonyl)-4,4′-bis(1-propynyl)biphenyls by diastereomeric encapsulation through the asymmetric suppression of rotation around the axis of the prochiral biphenyl moiety.

Introduction

Supramolecular capsules constructed by self-assembly of preorganized modular subunits provide an isolated nanospace.[1] Guest molecules confined in an isolated nanospace often show unique properties that are not observed in their free forms. Encapsulation of guest molecules in the capsules can be used for various applications such as separation techniques, capture and containment of hazardous chemicals, stabilization of reactive intermediates, catalysts, and sensing techniques.[1,2] Self-assembled capsules based on metal-coordination bonds have been extensively studied.[3-6]

Self-sorting has been defined as high-fidelity recognition of self from nonself within complex mixtures.[7] Self-sorting during self-assembled capsule formation through selection between homomeric assembly (narcissistic self-sorting or self-recognition) and heteromeric assembly (social self-sorting or self-discrimination) is an interesting topic in supramolecular chemistry, with a view to mimicking biological processes.[7-12] In almost all cases, selective formation of homomeric- or heteromeric-assembled capsules has depended on the structural demands of the modular subunits. However, control of selective formation between homomeric- and heteromeric-assembled capsules depending on guest encapsulation is almost unprecedented.[8a,b,9a]

As another topic, encapsulation strategies that use covalently bound and self-assembled capsules enable effective protection of reactive compounds against chemical or photochemical reactions.[13-16] *trans*-Azobenzene is a well-known photoresponsive molecule that undergoes *trans*-to-*cis* and *cis*-to-*trans* photoisomerizations upon UV and visible light irradiation, respectively. Upon UV light irradiation, the encapsulated *trans*-azobenzene is usually released from self-assembled capsules because of the *trans*-to-*cis* photoisomerization;[17] indeed, the preservation of *trans*-azobenzene encapsulated in self-assembled capsules upon UV light irradiation is without precedent.[16e]

Chiral capsules are another interesting topic in supramolecular nanospace chemistry. Chiral molecular recognition of a racemic guest upon encapsulation in chiral capsules has been studied extensively.[11a,18,19] In a type of twisted

capsule composed of north and south hemispheres, it is known that the equilibrium between (*P*)- and (*M*)-twistomers can be controlled either by the introduction of a chiral group onto a racemic self-assembled capsule[19b] or by the encapsulation of a chiral guest into a racemic self-assembled capsule.[6f,g,20] Chiral induction of a prochiral guest upon encapsulation in a chiral capsule would also be important for supramolecular nanospace chemistry[21] because such an encapsulation design is related to asymmetric capsular catalysts[22] and to the emergence of novel stereoisomerisms.[23]

Calix[4]resorcinarene-based tetrafunctionalized cavitands possess a bowl-shaped electron-rich aromatic cavity. They have been widely used as scaffolds for covalently bound and self-assembled capsules.[1c] Previously, we reported that a 2:4 mixture of tetra(4-pyridyl)cavitand (**3**) and Pd(dppp)$(OTf)_2$ in $CDCl_3$ gives a complex mixture, whereas the components of a 2:4 mixture of tetrakis(4-pyridylethynyl)cavitand (**4**) and Pd(dppp)$(OTf)_2$ self-assemble into Pd–pyridyl (Pd–Npy) coordination homocapsule $\{\mathbf{4}_2\cdot[Pd(dppp)]_4\}^{8+}\cdot(TfO^-)_8$ (**C4**) (Chart 1).[6c,d] However, we have not observed guest encapsulation of **C4** to date. Therefore, the characteristics of cavitand-based Pd–Npy coordination capsules upon guest encapsulation have remained unclear. The present work is concerned with a combination of expanded tetra(4-pyridyl)cavitand derivatives, i.e., tetrakis[4-(4-pyridyl)phenyl]cavitand (**1**)[24] or tetrakis[4-(4-pyridyl)phenylethynyl]cavitand (**2**), and Pd(dppp)$(OTf)_2$ (Chart 1). Our attention has focused on what functionalities (features) are exhibited by Pd–Npy coordination capsules that are composed of cavitand **1** or **2**. Here, we conducted a comprehensive study of cavitand-based Pd–Npy coordination capsules. We report (1) the formation of homocapsules $\{\mathbf{1}_2\cdot[Pd(dppp)]_4\}^{8+}\cdot(TfO^-)_8$ (**C1**) and $\{\mathbf{2}_2\cdot[Pd(dppp)]_4\}^{8+}\cdot(TfO^-)_8$ (**C2**) and a heterocapsule $\{\mathbf{1}\cdot\mathbf{2}\cdot[Pd(dppp)]_4\}^{8+}\cdot(TfO^-)_8$ (**C3**), (2) their guest-encapsulation ability, and (3) the control of self-sorting on homo- or heterocapsule selection by guest-induced encapsulation. We also describe applications of Pd–Npy coordination capsules with the use of **1** such as (4) usability of capsule **C1** as a guard nanocontainer for a photoresponsive guest and (5) the formation of a chiral capsule $\{\mathbf{1}_2\cdot[Pd((R)\text{-BINAP})]_4\}^{8+}\cdot(TfO^-)_8$ (**C5**) with the use of Pd((*R*)-BINAP)$(OTf)_2$ in place of Pd(dppp)$(OTf)_2$, wherein **C5** induces supramolecular chirality with respect to prochiral biphenyl guests by diastereomeric encapsulation.

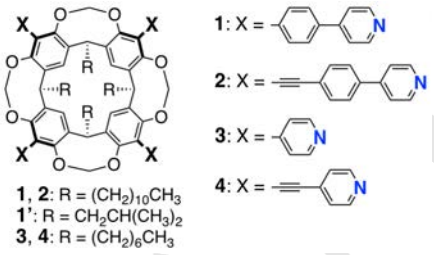

Chart 1. Structures of cavitands **1**–**4**.

Results and Discussion

Formation of homocapsules C1 and C2

Pd(dppp)$(OTf)_2$ has limited solubility in $CDCl_3$; however, a 2:4 mixture of tetrakis[4-(4-pyridyl)phenyl]cavitand (**1**, 2 mM) and Pd(dppp)$(OTf)_2$ in $CDCl_3$ becomes soluble at 25 °C after heating the mixture at 50 °C for 1 h. The ^{1}H NMR spectrum of the mixture showed the formation of a highly symmetrical single species, indicative of a homocapsule $\{\mathbf{1}_2\cdot[Pd(dppp)]_4\}^{8+}\cdot(TfO^-)_8$ (**C1**) through Pd–Npy coordination bonds (Scheme 1a), and the complete disappearance of the signals of free **1** and free Pd(dppp)$(OTf)_2$ (Figure 1c vs. Figures 1a, b and Figure S3). The signal assignments of **C1** were supported by the ^{1}H–^{1}H COSY spectrum (Figure S4). The signals of the pyridyl α-proton and the outer proton of the methylene-bridge rim ($O\text{-}CH_{in}H_{out}\text{-}O$) of **C1** were shifted downfield by 0.40 and 0.10 ppm, respectively, and the signals of the pyridyl β-proton and the inner proton of the methylene-bridge rim of **C1** were shifted upfield by 0.30 and 0.12 ppm, respectively, relative to those of free **1**. The large downfield shift of the pyridyl α-proton of the subunit **1** ($\Delta\delta$ = 0.40 ppm) indicates the formation of the Pd–Npy coordination bond.[6c,d] Further evidence for the formation of **C1** was provided by the ESI-TOF-MS spectrum and guest encapsulation experiments (vide infra).

A 2:4 mixture of tetrakis[4-(4-pyridyl)phenylethynyl]cavitand (**2**; 2 mM) and Pd(dppp)$(OTf)_2$ in $CDCl_3$ also becomes soluble at 25 °C after heating the mixture at 50 °C for 1 h. The ^{1}H NMR spectrum of the mixture showed the formation of a highly symmetrical single species, indicative of a homocapsule $\{\mathbf{2}_2\cdot[Pd(dppp)]_4\}^{8+}\cdot(TfO^-)_8$ (**C2**) through Pd–Npy coordination bonds (Figure 1e vs. Figure 1d, Scheme 1b, and Figures S5 and S6). The signal of the pyridyl α-proton of **C2** was shifted downfield by 0.39 ppm, and the signals of the pyridyl β-proton and the inner and outer protons of the methylene-bridge rim of **C2** were shifted upfield by 0.25, 0.11, and 0.06 ppm, respectively, relative to those of free **2**.[6c,d] Further evidence for the formation of **C2** was provided by the ESI-TOF-MS spectrum (vide infra).

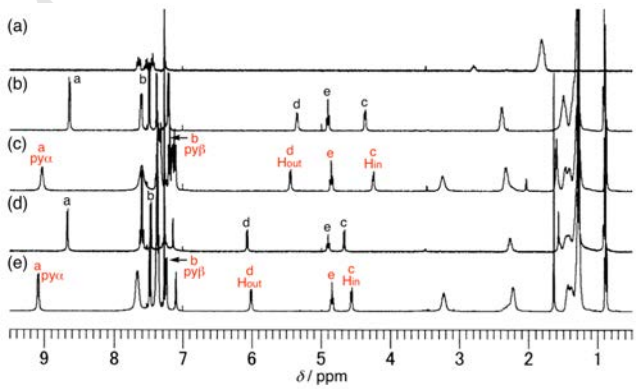

Figure 1. Association behavior of cavitands **1** or **2** with Pd(dppp)$(OTf)_2$ monitored by ^{1}H NMR (400 MHz, $CDCl_3$, 298 K): (a) Pd(dppp)$(OTf)_2$ alone, (b) **1** alone (2 mM), (c) capsule **C1** (after heating a mixture of **1** (2 mM) and Pd(dppp)$(OTf)_2$ (4 mM) at 50 °C for 1 h), (d) **2** alone (2 mM), and (e) capsule **C2** (after heating a mixture of **2** (2 mM) and Pd(dppp)$(OTf)_2$ (4 mM) at 50 °C for 1 h). The signals marked "a–e" are assigned in Scheme 1. The representative signals of free species and complexes are shown in black and red, respectively.

Guest encapsulation in homocapsules C1 and C2

Capsule **C1** encapsulates one guest molecule such as bis(4-acetoxyphenyl)acetylene (**G1**) or 4,4′-bis(1-propynyl)biphenyl (**G2**) to form guest-encapsulating capsule **G@C1** (Scheme 1a).

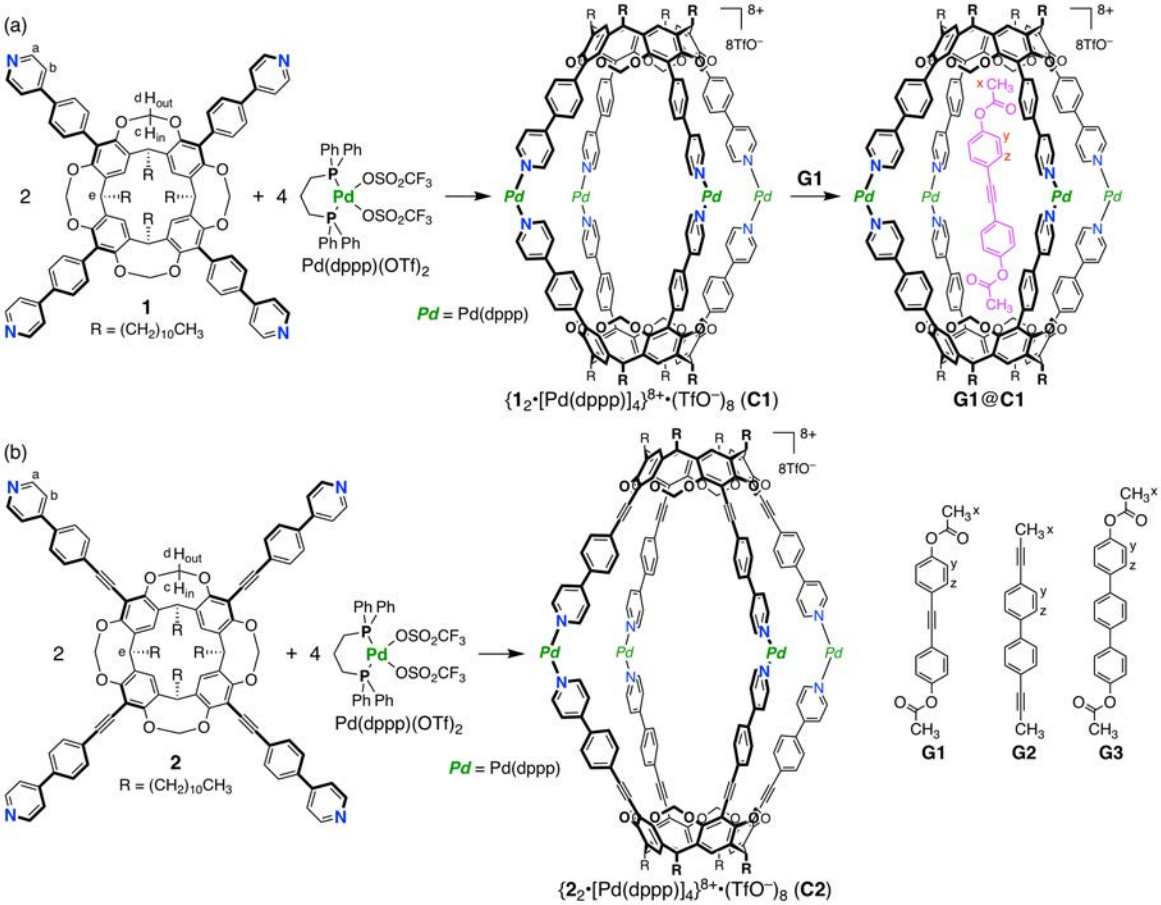

Scheme 1. (a) Self-assembly of a 2:4 mixture of cavitand **1** and Pd(dppp)(OTf)$_2$ into homocapsule **C1** and its guest encapsulation; (b) self-assembly of a 2:4 mixture of cavitand **2** and Pd(dppp)(OTf)$_2$ into homocapsule **C2**.

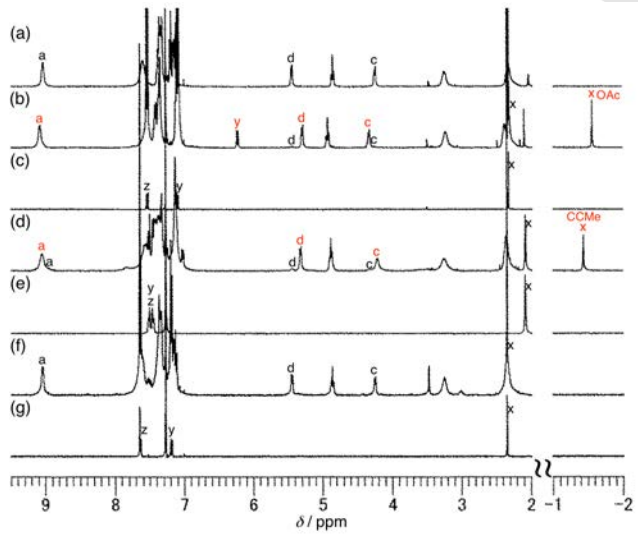

Figure 2. Association behavior of capsule **C1** or **C2** with guests **G1**~**G3** monitored by ^{1}H NMR (400 MHz, $CDCl_3$, 298 K): (a) **C1** alone (1 mM), (b) **G1@C1** ([**C1**] = 1 mM + [**G1**] = 10 mM), (c) **G1** alone, (d) **G2@C1** ([**C1**] = 1 mM + [**G2**] = 2 mM), (e) **G2** alone, (f) [**C1**] = 1 mM + [**G3**] = 6 mM, and (g) **G3** alone. The signals marked "a–e" and "x–z" are assigned in Scheme 1. The representative signals of free species and complexes are shown in black and red, respectively.

The ^{1}H NMR spectrum of a 1:10 mixture of **C1** (1 mM; [**1**] = 2 mM and [Pd(dppp)(OTf)$_2$] = 4 mM) and **G1** (10 mM) in $CDCl_3$ at 298 K showed formation of **G1@C1** (Figures 2b and S7). The ^{1}H NMR signals of **G1@C1**, free **C1**, and free **G1** were independently observed. This result indicates that one molecule of **G1** is encapsulated in **C1** and that the exchange of **G1** in and out of **C1** is slow on the NMR time-scale. The ^{1}H NMR chemical shift changes of the signals of the encapsulated **G1** relative to those of free **G1** ($\Delta\delta = \delta_{\text{encapsulated-guest}} - \delta_{\text{free-guest}}$) were –3.88 ppm for the protons of the acetoxy groups (signal-x, OAc) at the *para*-positions and –0.87 ppm for the aromatic *meta*-proton (signal-y). The very large upfield shift of the acetoxy groups of the encapsulated **G1** is due to the shielding effect of the aromatic cavity ends of **C1**. This result indicates that the acetoxy groups of **G1** are oriented toward both aromatic cavity ends of **C1** (Scheme 1a) to maximize CH···π interaction between the methyl moiety of the acetoxy group of **G1** and the electron-rich aromatic cavity of the subunit **1**. Based on the integration ratios of the three species as a function of concentration, the association constant (K_a) of **C1** with **G1** was estimated to be 2.27×10^3 M^{-1} in $CDCl_3$ at 298 K.

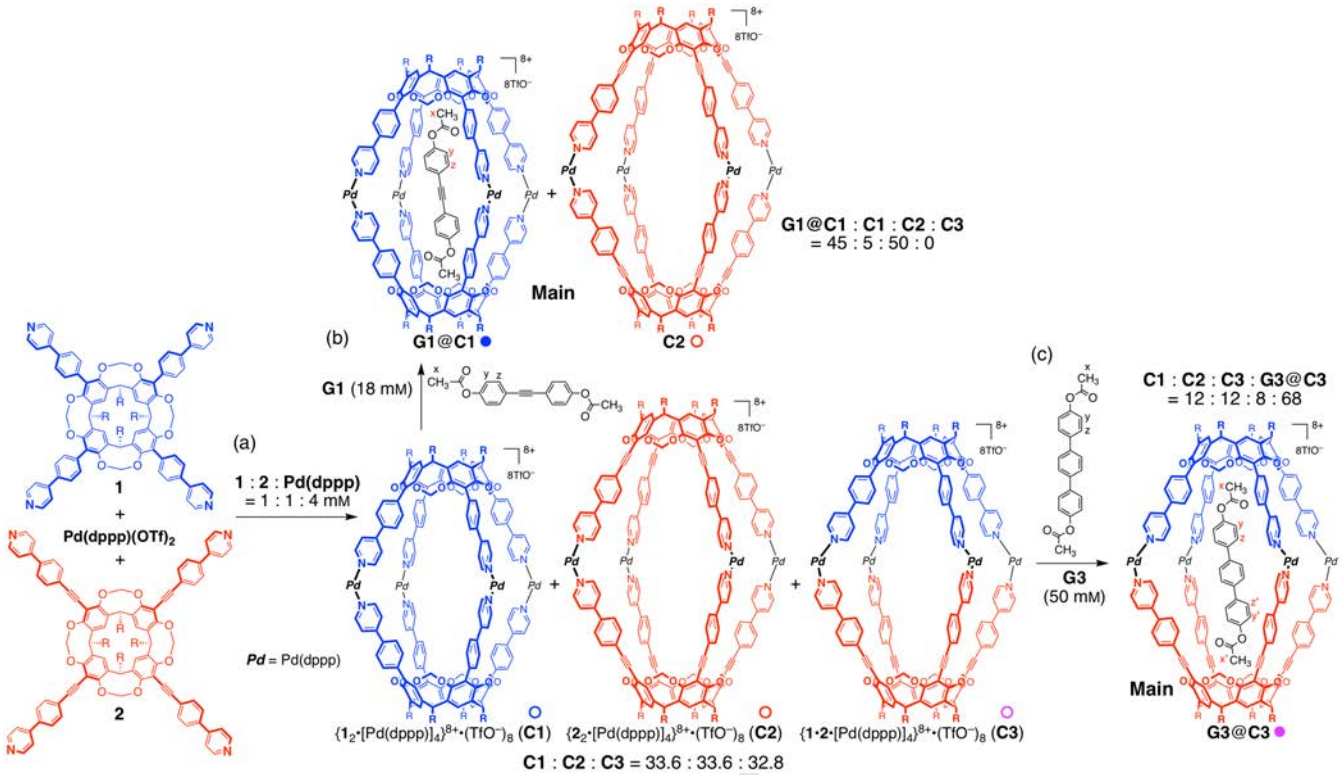

Scheme 2. Control of self-sorting by guest encapsulation: (a) self-assembly of a 1:1:4 mixture of cavitand **1**, cavitand **2**, and Pd(dppp)(OTf)$_2$ into a mixture of homocapsules **C1**, **C2**, and heterocapsule **C3**; (b) upon addition of **G1**, thermodynamic equilibration shift of a mixture of **C1**, **C2**, and **C3** into a **G1@C1**-enriched and **C2**-enriched mixture; (c) upon addition of **G3**, thermodynamic equilibration shift of a mixture of **C1**, **C2**, and **C3** into a **G3@C3**-enriched mixture.

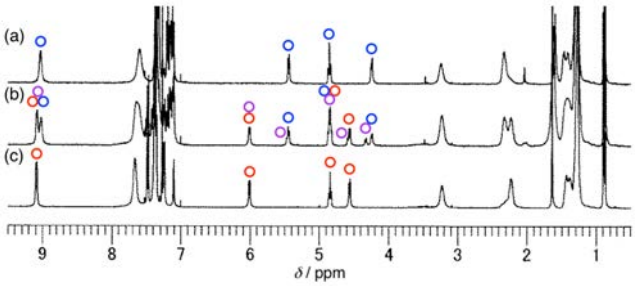

Figure 3. ^{1}H NMR spectra (400 MHz, $CDCl_3$, 298 K) of (a) homocapsule **C1** alone (1 mM), (b) a mixture of **C1**, **C2**, and heterocapsule **C3** (after heating a mixture of **1** (1 mM), **2** (1 mM), and Pd(dppp)(OTf)$_2$ (4 mM) at 50 °C for 1 h), and (c) homocapsule **C2** alone (1 mM). The representative signals of **C1**, **C2**, and **C3** are marked with blue, red, and purple open circles, respectively. See also Scheme 2a.

The ^{1}H NMR spectrum of a 1:2 mixture of **C1** (1 mM) and **G2** (2 mM) in $CDCl_3$ at 298 K showed formation of **G2@C1** (Figures 2d and S8). The ^{1}H NMR signals of **G2@C1**, free **C1**, and free **G2** were independently observed. The $\Delta\delta$ value for the protons of the 1-propynyl groups (signal-x, CCMe) at the *para*-positions was –3.52 ppm. This result indicates that the 1-propynyl groups of **G2** are oriented toward both aromatic cavity ends of **C1**. The K_a value of **C1** with **G2** was estimated to be 9.53×10^3 M^{-1} in $CDCl_3$ at 298 K.

Capsule **C1** is sensitive to the guest molecular length for guest encapsulation, and does not encapsulate molecules such as 4,4′′-diacetoxy-*p*-terphenyl (**G3**), which do not fit the cavity size of **C1** (Figures 2f and S9). The cavity size of **C2** is larger than that of **C1**. Capsule **C2** does not encapsulate **G1**, **G2**, or **G3** because the molecular sizes of these guests are small relative to the cavity size of **C2** (Figure S9). At this stage, we have not been able to observe guest encapsulation of **C2**.[25]

Self-sorting in capsule formation: homomeric vs. heteromeric capsule

Self-sorting through selection between homomeric assembly and heteromeric assembly is an interesting topic. However, control of selective formation between homomeric and heteromeric assembled capsules depending on guest encapsulation is almost unprecedented.[8a,b,9a]

A 1:1:4 mixture of **1** (1 mM), **2**, and Pd(dppp)(OTf)$_2$ in $CDCl_3$ becomes soluble at 25 °C after heating the mixture at 50 °C for 1 h. The ^{1}H NMR spectrum of the mixture showed the expected signals for homocapsules **C1** and **C2**, and signals for the formation of a new species also appeared at 4.33 ppm (independent), 4.58 ppm partially overlapped with the signal of the inner proton (H_{in}) of the methylene-bridge rim (O-$CH_{in}H_{out}$-O) of **C2**, and 5.46 ppm partially overlapped with the signal of the outer proton (H_{out}) of the methylene-bridge rim of **C1** (Figures 3b and S10), although other signals of a new species were completely overlapped with the signals of **C1** or **C2**. Based on comparisons of chemical shifts and integration ratios of the ^{1}H NMR signals of the new species with those of **C1** and **C2**, it is suggested that the

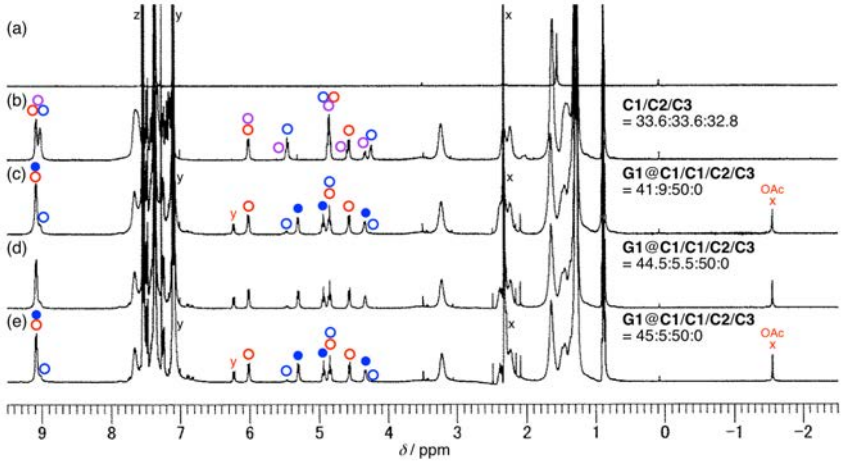

Figure 5. Association behavior of a mixture of **C1**, **C2**, and **C3** with **G1** monitored by ^{1}H NMR (400 MHz, $CDCl_3$, 298 K): (a) **G1** alone; (b) a mixture of **C1**, **C2**, and **C3** after heating a mixture of **1** (1 mM), **2** (1 mM), and Pd(dppp)$(OTf)_2$ (4 mM) at 50 °C for 1 h; after heating a mixture of **C1**, **C2**, **C3**, and **G1** (6–18 mM) at 50 °C for 1 h: [**G1**] = (c) 6 mM, (d) 12 mM, and (e) 18 mM. The representative signals of **G1@C1**, **C1**, **C2**, and **C3** are marked with blue solid circle, and blue, red, and purple open circles, respectively. The signals "x and y" of encapsulated **G1** and those of free **G1** are shown in red and black, respectively. See also Scheme 2b.

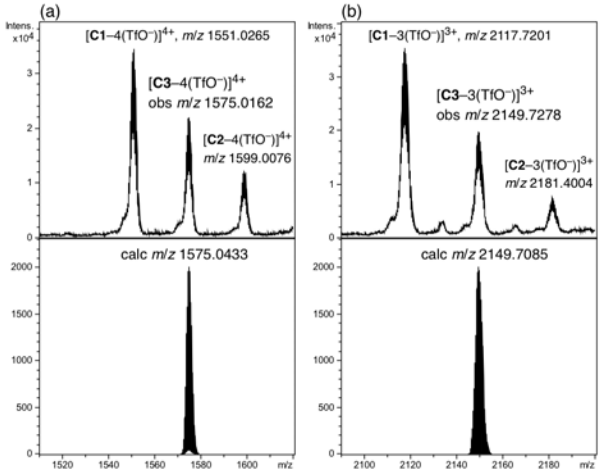

Figure 4. ESI-TOF-MS spectrum of a 1:1:4 mixture of **1** (0.01 mM), **2**, and Pd(dppp)$(OTf)_2$ (a mixture of capsules **C1**, **C2**, and **C3**) in $CHCl_3$ (capillary = –3500 V and ion source temperature = 34 °C): (a) top: observed spectrum of [M – 4(TfO$^-$)]$^{4+}$ (M = **C1**, **C2**, and **C3**), bottom: calculated spectrum of [**C3** – 4(TfO$^-$)]$^{4+}$; (b) top: observed spectrum of [M – 3(TfO$^-$)]$^{3+}$ (M = **C1**, **C2**, and **C3**), bottom: calculated spectrum of [**C3** – 3(TfO$^-$)]$^{3+}$. See also Figure S12.

new species is a hetero-capsule {**1**·**2**·[Pd(dppp)]$_4$}$^{8+}$·(TfO$^-$)$_8$ (**C3**) composed of **1**, **2**, and Pd(dppp)$(OTf)_2$ in a 1:1:4 mole ratio (Scheme 2a). The three aforementioned signals of **C3** were assigned to the H_{in} of the subunit-**1**, the H_{in} of the subunit-**2**, and the H_{out} of subunit-**1**, the detail of which is shown in Figure 7a (vide infra). Based on the signal integration ratios of the H_{in} of the methylene-bridge rims of **C1**, **C2**, and **C3**, the product ratio of **C1**, **C2**, and **C3** was estimated to be 1:1:0.98 (Figure 3b). This product ratio remained unchanged after 24 h at room temperature and also after additional heating at 50 °C for 12 h (Figure S11), indicating that the thermodynamic equilibration between **C1**, **C2**, and **C3** was reached after initial heating the mixture at 50 °C for 1 h (Figure 3b). The product ratio of homocapsules **C1** and **C2** is inevitably 1:1, when **1**, **2**, and Pd(dppp)$(OTf)_2$ are mixed in a 1:1:4 mole ratio. The formation of **C1** and **C2** was preferred, because **C1** is thermodynamically most stable among **C1**, **C2**, and **C3**. Concrete evidence for the formation of **C3** was provided by the ESI-TOF-MS spectrum of the mixture (Figures 4 and S12), wherein the molecular ion peaks of **C3** were observed at *m/z* 2149.7278 [**C3** – 3(TfO$^-$)]$^{3+}$ (calcd 2149.7085) and 1575.0162 [**C3** – 4(TfO$^-$)]$^{4+}$ (calcd 1575.0433), in addition to those of **C1** at *m/z* 2117.7201 [**C1** – 3(TfO$^-$)]$^{3+}$ (calcd 2117.7084) and 1551.0265 [**C1** – 4(TfO$^-$)]$^{4+}$ (calcd 1551.0432) and those of **C2** at *m/z* 2181.4004 [**C2** – 3(TfO$^-$)]$^{3+}$ (calcd 2181.7086) and 1599.0076 [**C2** – 4(TfO$^-$)]$^{4+}$ (calcd 1599.0433). Further evidence for the formation of **C3** was supported by guest-encapsulation experiments (vide infra).

As mentioned above, guest **G1** is encapsulated in homocapsule **C1**, but not **C2**. Figure 5 shows the ^{1}H NMR spectra of the mixture upon addition of **G1** to the equilibrated mixture of **C1**, **C2**, and **C3** (1:1:0.98) derived from a 1:1:4 mixture of **1** (1 mM), **2**, and Pd(dppp)$(OTf)_2$ in $CDCl_3$ as described above. Upon addition of **G1** (6 mM), the signals of guest-encapsulating **G1@C1** and free **C2** increased with a decrease of those of free **C1** and with complete disappearance of those of **C3** (Figure 5c). The product ratio of **G1@C1**, **C1**, **C2**, and **C3** was shifted to 41:9:50:0, wherein a thermodynamic equilibration was shifted most favorably toward formation of **G1@C1** through **G1**-induced stabilization of **C1** by encapsulation (Scheme 2b). Upon further addition of **G1** (18 mM in total), the product ratio of **G1@C1**, **C1**, **C2**, and **C3** changed to 45:5:50:0 (Figures 5e and S13). Thus, selective formation of homocapsules **C1** and **C2** was achieved upon addition of **G1**. Guest **G2** also induced selective formation of the homocapsules. Upon addition of **G2** (18 mM) to the mixture of **C1**, **C2**, and **C3** (1:1:0.98) described above, the product ratio of **G2@C1**, **C1**, **C2**, and **C3** was shifted to 50:0:50:0 (Figure S14).

As noted above, homocapsules **C1** and **C2** do not encapsulate **G3** because the cavity sizes of **C1** and **C2** are too small or large, respectively, relative to the molecular size of **G3**. The cavity size of heterocapsule **C3** is between those of

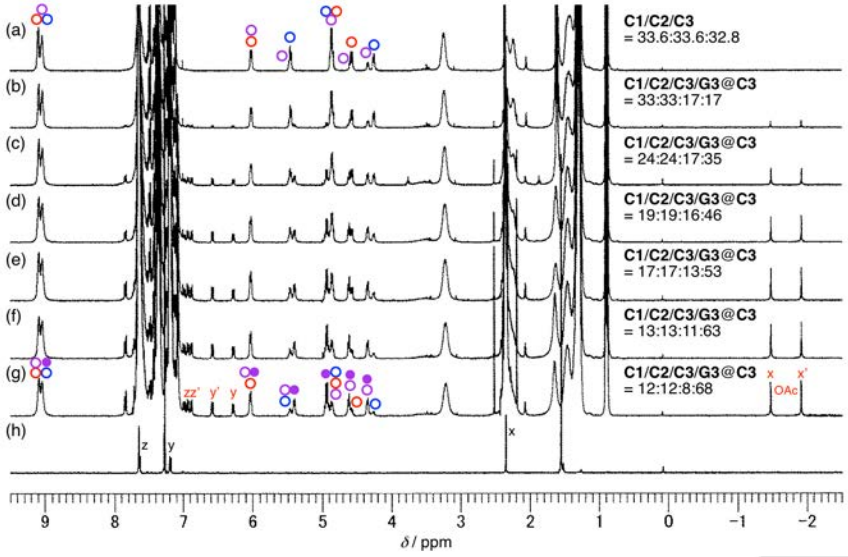

Figure 6. Association behavior of a mixture of **C1**, **C2**, and **C3** with **G3** monitored by ^{1}H NMR (400 MHz, $CDCl_3$, 298 K): (a) a mixture of **C1**, **C2**, and **C3** after heating a mixture of **1** (1 mM), **2** (1 mM), and Pd(dppp)$(OTf)_2$ (4 mM) at 50 °C for 1 h; after heating a mixture of **C1**, **C2**, **C3**, and **G3** (5–50 mM) at 50 °C for 1 h: [**G3**] = (b) 6 mM, (c) 15 mM, (d) 20 mM, (e) 30 mM, (f) 40 mM, and (g) 50 mM; and (h) **G3** alone. The representative signals of **G3@C3**, **C1**, **C2**, and **C3** are marked with purple solid circle, and blue, red, and purple open circles, respectively. The signals "x–z" and "x′–z′" shown in red indicate the encapsulated **G3** oriented to the subunits-**1** and -**2** of **C3**, respectively. See also Scheme 2c.

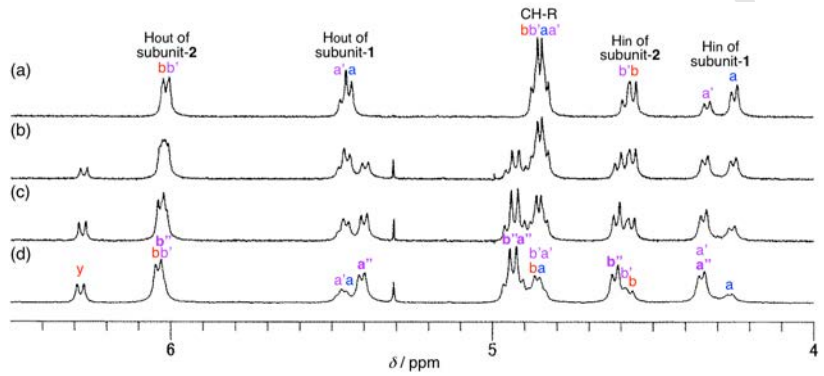

Figure 7. Expanded spectra of (a) Figure 6a, (b) Figure 6c, (c) Figure 6e, and (d) Figure 6g in the region of the inner (H_{in}) and outer (H_{out}) protons of the methylene-bridge rims (O-$CH_{in}H_{out}$-O) and the basal CH of side chain R of capsules. The signals marked "a" and "b" indicate **C1** and **C2**, respectively. The signals marked "a′" and "b′" indicate the subunits-**1** and -**2** of **C3**, respectively. The signals marked "a′′" and "b′′" indicate the subunits-**1** and -**2** of **G3@C3**, respectively.

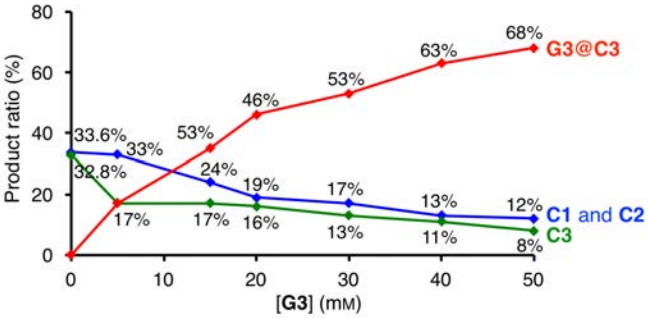

Figure 8. Plots of the product ratio of **G3@C3**, **C1**, **C2**, and **C3** as a function of [**G3**], based on the ^{1}H NMR data of Figure 6.

homocapsules **C1** and **C2**. As a result, it was found that heterocapsule **C3** selectively encapsulates **G3** to form **G3@C3** (Scheme 2c). Figure 6 shows the ^{1}H NMR spectra of the mixture upon addition of **G3** to the equilibrium mixture of **C1**, **C2**, and **C3** (1:1:0.98) derived from a 1:1:4 mixture of **1** (1 mM), **2**, and Pd(dppp)$(OTf)_2$ in $CDCl_3$, as described above. Figure 7 shows the expanded spectra of Figure 6 in the region of the inner (H_{in}) and outer (H_{out}) protons of the methylene-bridge rims (O-$CH_{in}H_{out}$-O) of capsules. The signals of **C1**, **C2**, and **C3** were assigned as shown in Figures 7a and 6a. The signals-a indicate the H_{in} at 4.25 ppm and the H_{out} at 5.45 ppm (partially overlap) of homocapsule **C1**, and the signals-b indicate the H_{in} at 4.56 ppm (partially overlap) and the H_{out} at 6.02 ppm (overlap) of homocapsule **C2**. For heterocapsule **C3**, the signals-a′ indicate the H_{in} at 4.33 ppm and the H_{out} at 5.46 ppm (partial overlap) of the subunit-**1**, and the signals-b′ indicate the H_{in} at 4.58 ppm (partial overlap) and the

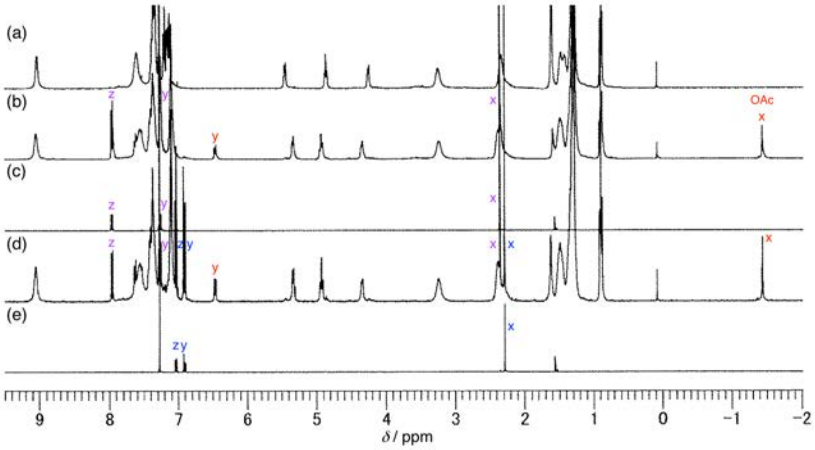

Figure 9. ^{1}H NMR spectra (400 MHz, $CDCl_3$, 298 K) of (a) **C1** alone (1 mM), (b) *trans*-**G4**@**C1** ([**C1**] = 1 mM + [*trans*-**G4**] = 3 mM), (c) *trans*-**G4** alone (3 mM), (d) after 350 nm irradiation of a mixture of **C1** (1 mM) and *trans*-**G4** (3 mM) for 60 min, and (e) after 350 nm irradiation of *trans*-**G4** (3 mM) for 60 min. The signals "x–z" shown in red, purple, and blue indicate *trans*-**G4** encapsulated in **C1**, free *trans*-**G4**, and free *cis*-**G4**, respectively, which are assigned in Scheme 3.

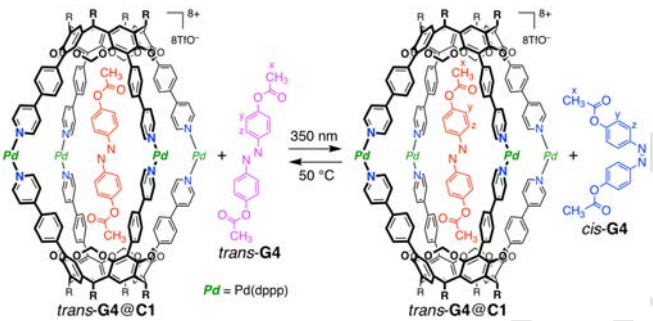

Scheme 3. Almost no photoisomerization of *trans*-**G4** encapsulated in **C1**.

H_{out} at 6.02 ppm (overlap) of the subunit-**2**. For guest-encapsulating heterocapsule **G3**@**C3**, the signals-a′′ indicate the H_{in} at 4.35 ppm (overlap) and the H_{out} at 5.41 ppm of the subunit-**1**, and the signals-b′′ indicate the H_{in} at 4.62 ppm (partial overlap) and the H_{out} at 6.04 ppm (overlap) of subunit-**2**, which were assigned based on 2D NOESY experiments (Figure S15) on the sample (Figures 7d and 6g). Upon increasing the amount of **G3**, new signals indicating **G3**@**C3** increased with decreases of signals for free **C1**, free **C2**, and free **C3** (Figures 6 and 7), wherein a thermodynamic equilibration was shifted most favorably toward formation of **G3**@**C3** through **G3**-induced stabilization of **C3** by encapsulation. Upon further addition of **G3** (50 mM in total), the product ratio of **C1**, **C2**, **C3**, and **G3**@**C3** reached 12:12:8:68 (Figures 6g and 7d). Figure 8 shows the plots of the product ratio of **G3**@**C3**, **C1**, **C2**, and **C3** as a function of [**G3**].

As the electronic environment of the subunit-**1** differs from that of the subunit-**2** in heterocapsule **C3**, the **G3** encapsulated in **C3** is desymmetrized. Thus, the ^{1}H NMR signals of **G3** encapsulated in **C3** appeared as two sets of signals (Figure 6). Representative ^{1}H NMR signals of **G3** encapsulated in **C3** appeared at –1.48 ppm ($\Delta\delta$ = –3.83 ppm) and –1.92 ppm ($\Delta\delta$ = –4.27 ppm) for the acetoxy protons (signal-OAc, x and x′) at the *para*-positions and at 6.58 ppm ($\Delta\delta$ = –0.61 ppm) and 6.28 ppm ($\Delta\delta$ = –0.91 ppm) for the aromatic *meta*-protons (signals-y′ and y). In other words, this **G3**-encapsulation behavior in a capsule provides definitive evidence for the formation of heterocapsule **C3**. The very large upfield shift of the acetoxy protons of the encapsulated **G3** indicates that the acetoxy groups of **G3** are oriented toward both aromatic cavity ends of **C3**. The 2D NOESY spectrum (Figure S15b) of the sample (Figures 6g and 7d) disclosed the orientation of **G3** encapsulated in **C3**. The acetoxy proton signal-x of –1.48 ppm ($\Delta\delta$ = –3.83 ppm) showed the NOE correlations to the signals-a′′ of H_{in} and H_{out} of the subunit-**1**; i.e., the acetoxy group-x is oriented to the subunit-**1**. On the other hand, the more upfield-shifted acetoxy proton signal-x′ of –1.92 ppm ($\Delta\delta$ = –4.27 ppm) showed the NOE correlations to the signals-b′′ of H_{in} and H_{out} of the subunit-**2**; i.e., the acetoxy group-x′ is oriented to the subunit-**2**. The NOE correlations were also observed between the aromatic proton signal-y′ of **G3** and the signals-b′′ of H_{in} of the subunit-**2**, and between the aromatic proton signal-y′ and the aromatic proton signal-z′ of **G3**.

The **G3**-encapsulation in the equilibrium mixture of **C1**, **C2**, and **C3** was investigated in more detail. The ^{1}H NMR spectrum just after addition of **G3** (40 mM) at room temperature to the equilibrium mixture of **C1**, **C2**, and **C3** (33.6:33.6:32.8) derived from a 1:1:4 mixture of **1** (1 mM), **2**, and $Pd(dppp)(OTf)_2$, showed the product ratio of **C1**/**C2**/**C3**/**G3**@**C3** = 26:26:4:44 (Figure S16b). The ^{1}H NMR spectrum of this mixture after 24 h at 25 °C indicated a change in the product ratio of **C1**/**C2**/**C3**/**G3**@**C3** to 13:13:11:63 (Figure S16c). However, the product ratio remained unchanged after additional heating of this mixture at 50 °C for 12 h (Figure S16d). These results suggest that the encapsulation of **G3** in **C3** is relatively fast, and the equilibrium shift of **C1** and **C2** toward **C3** is relatively slow. This product ratio was the same as that of the sample after heating the initial mixture at 50 °C for 1 h (Figure 6f).

Capsule C1 as a guard nanocontainer for *trans*-4,4′-diacetoxyazobenzene

In the ^{1}H NMR study (Figures 9b and S17), capsule **C1** also encapsulates *trans*-4,4′-diacetoxyazobenzene (*trans*-**G4**) to form

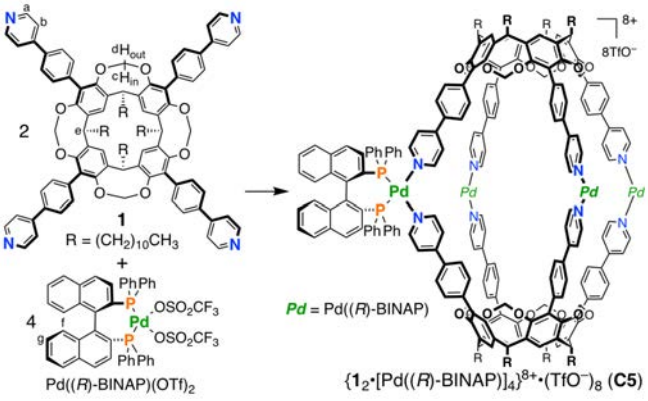

Scheme 4. Self-assembly of a 2:4 mixture of cavitand **1** and Pd((*R*)-BINAP)(OTf)$_2$ into chiral capsule **C5**.

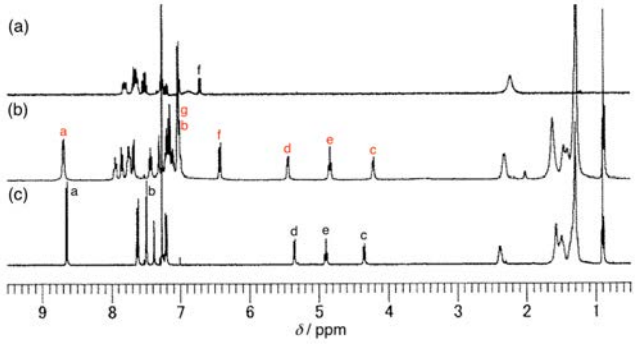

Figure 10. Association behavior of cavitand **1** with Pd((*R*)-BINAP)(OTf)$_2$ monitored by ^{1}H NMR (400 MHz, $CDCl_3$, 298 K): (a) Pd((*R*)-BINAP)(OTf)$_2$ alone, (b) chiral capsule **C5** (after heating a mixture of **1** (2 mM) and Pd((*R*)-BINAP)(OTf)$_2$ (4 mM) at 50 °C for 1 h), and (c) **1** alone (2 mM). The signals marked "a–g" are assigned in Scheme 4. The representative signals of free species and **C5** are shown in black and red, respectively.

trans-**G4**@**C1** with $\Delta\delta$ = –3.80 ppm for the acetoxy proton signal (δ = –1.44 ppm) and K_a = 14.0 × 10^3 M^{-1} in $CDCl_3$ at 298 K.

Irradiation of *trans*-**G4** (3 mM) in $CDCl_3$ with 350 nm light[26] resulted in the photoisomerization to *cis*-**G4**, wherein the ^{1}H NMR signals of *trans*-**G4** (δ = 7.96, 7.26, and 2.36 ppm) decreased with increasing signal intensity for *cis*-**G4** (δ = 7.04, 6.91, and 2.29 ppm) (Figure 9c vs. Figures 9e and S18). The photostationary state was reached within 60 min (*trans*-**G4**/*cis*-**G4** = 2:98). In marked contrast, the *trans*-**G4** encapsulated in **C1**, derived from a 1:3 mixture of **C1** (1 mM) and *trans*-**G4** (3 mM) in $CDCl_3$, underwent almost no photoisomerization to *cis*-**G4** (Figures 9d and S19). Upon 350 nm irradiation for 60 min, the encapsulation ratio of *trans*-**G4** encapsulated in **C1** remained almost unchanged (only 6% reduction of encapsulation), although excess amount of *trans*-**G4**, which was not encapsulated in **C1**, photoisomerized to *cis*-**G4** (Scheme 3). The acetoxy groups of *trans*-**G4** encapsulated in **C1** are oriented toward both aromatic cavity ends of **C1** ($\Delta\delta$ = –3.80 ppm), leading to tight encapsulation of *trans*-**G4**. As a result, confined space of *trans*-**G4**@**C1** would interfere with geometrical change in the transition state of *trans*-to-*cis* photoisomerization of *trans*-**G4**. Thus, capsule **C1** serves as a guard nanocontainer for *trans*-**G4** to protect against the *trans*-to-*cis* photoisomerization of *trans*-**G4** by encapsulation in **C1**. Furthermore, this protection may be explained by the very slow exchange of *trans*-**G4** in and out of **C1**, in which the exchange cross-peak between the encapsulated and free *trans*-**G4** in the 2D NOESY spectrum was not observed even at 323 K (Figure S20), and/or overlap of UV–vis absorption bands between **C1** and *trans*-**G4** at 350 nm (Figure S21).

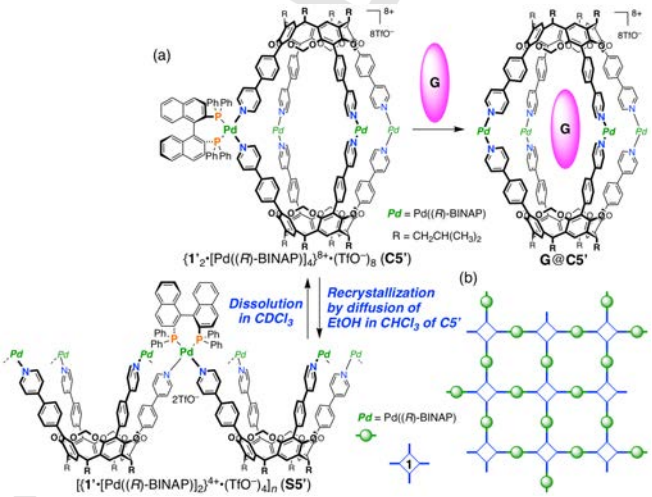

Figure 11. Schematic illustration of structural interconversion between (a) capsule **C5′** (R = $CH_2CH(CH_3)_2$) in solution and (b) an infinite 2D coordination-bonded network sheet structure **S5′** in the crystalline state.

Formation of chiral capsule C5

We found the formation of a chiral capsule {**1**$_2$·[Pd((*R*)-BINAP)]$_4$}$^{8+}$·(TfO$^-$)$_8$ (**C5**) with the use of Pd((*R*)-BINAP)(OTf)$_2$ in place of Pd(dppp)(OTf)$_2$.[27]

A 2:4 mixture of **1** (R = $(CH_2)_{10}CH_3$) (2 mM) and Pd((*R*)-BINAP)(OTf)$_2$ in $CDCl_3$ became soluble at 25 °C after heating the mixture at 50 °C for 1 h. The ^{1}H NMR spectrum of the mixture showed the formation of a highly symmetrical single species, indicative of a chiral capsule {**1**$_2$·[Pd((*R*)-BINAP)]$_4$}$^{8+}$·(TfO$^-$)$_8$ (**C5**) through Pd–Npy coordination bonds (Scheme 4), and the complete disappearance of the signals of free **1** and free Pd((*R*)-BINAP)(OTf)$_2$ (Figure 10b vs. Figure 10a, c). The signal assignments of **C5** were supported by the ^{1}H–^{1}H COSY spectrum (Figure S22). The signals of the pyridyl α-proton and the outer proton of the methylene-bridge rim (O-$CH_{in}H_{out}$-O) of **C5** were shifted downfield by 0.04 and 0.11 ppm, respectively, and the signals of the pyridyl β-proton and the inner proton of the methylene-bridge rim of **C5** were shifted upfield by 0.47 and 0.15 ppm, respectively, relative to those of free **1**. The very small downfield shift of the pyridyl α-proton and the relatively large upfield shift of the pyridyl β-proton of the subunit **1** of **C5**, compared with those of **C1**, suggest the shielding effect of the subunit (*R*)-BINAP. Further evidence for the formation of **C5** was supported by guest encapsulation experiments (vide infra).

Single crystals of the components of a 2:4 mixture of **1′** (R = $CH_2CH(CH_3)_2$) and Pd((*R*)-BINAP)(OTf)$_2$, suitable for X-ray diffraction analysis, were obtained by slow diffusion of EtOH into a $CHCl_3$ solution of {**1′**$_2$·[Pd((*R*)-BINAP)]$_4$}$^{8+}$·(TfO$^-$)$_8$ (**C5′**). However, surprisingly, the crystal structure was not the discrete capsule **C5′**, but was found to be an infinite two-dimensional Pd–Npy coordination-bonded porous network sheet structure

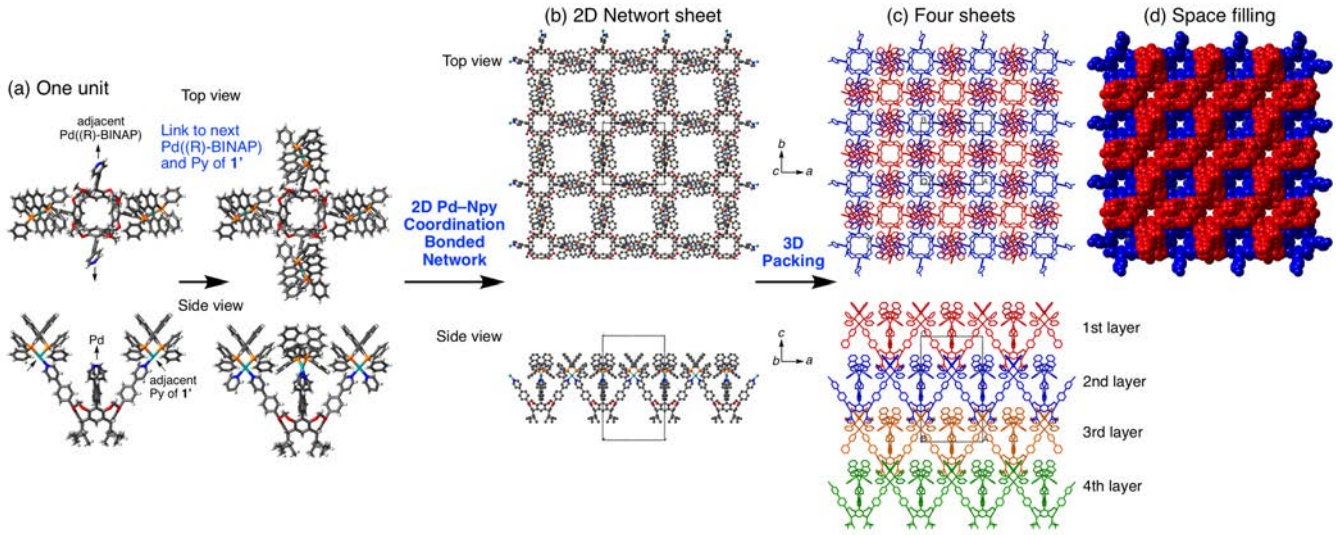

Figure 12. X-ray crystal structure of **S5′**: (a) one unit structure, (b) 2D coordination-bonded network sheet structure, (c) 3D packing structure (assembly of four sheets), and (d) its space filling representation. In Figure 12a, triflate ions are omitted for clarity. In Figures 12b–d, triflate ions and hydrogen atoms are omitted for clarity.

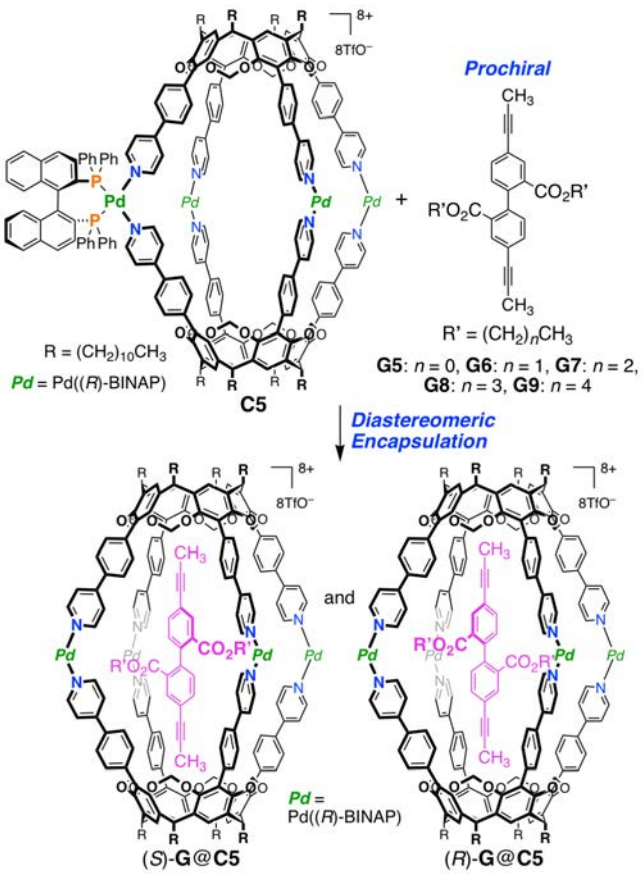

Scheme 5. Schematic illustration of diastereomeric encapsulation of prochiral biphenyl guests **G5**~**G9** in chiral capsule **C5**.

$[\{\mathbf{1'}\cdot[Pd((R)\text{-BINAP})]_2\}^{4+}\cdot(TfO^-)_4]_n$ (**S5′**) (Figure 11). Figure 12 shows the one-unit structure, 2D network sheet structure, and 3D packing structure of **S5′** in the crystal structure.[28] Crystal data and structural refinement of **S5′** are listed in Table S1, and an ORTEP view is shown in Figure S23A. Each **1′** is placed in the *ab* plane in a parallel fashion along the *c* axis, and is connected with Pd((*R*)-BINAP) by the Pd–Npy coordination bonds to form 2D coordination-bonded porous network sheet **S5′**, with square cavities of dimension ca. 8.4 Å × 8.4 Å including van der Waals radii (Figure 12a, b). The bond distances of Pd–N and Pd–P are 2.111 Å and 2.280 Å, respectively, and the bond angles of N–Pd–N, P–Pd–P, and N–Pd–P are 84.601°, 90.814°, and 92.907°, respectively. The adjacent 2D coordination-bonded porous network sheets of **S5′**, which are separated by 16.83 Å (1/2*c* of the unit cell) and are translated by 9.89 Å along the *a* axis (1/2*a* of the unit cell) and 9.89 Å along the *b* axis (1/2*b* of the unit cell), are layered in an offset manner (ABAB pattern) to give a 3D packing structure with chambers (but no channels) (Figure 12c, d). The ^{1}H NMR spectrum of a solution upon dissolving the single crystals of **S5′** in CD_2Cl_2 showed that single crystals of **S5′** include $CHCl_3$ and EtOH as cocrystal solvents in a ratio of $\{\mathbf{1'}\cdot[Pd((R)\text{-BINAP})]_2\}^{4+}\cdot(TfO^-)_4/CHCl_3/EtOH$ = 1:1:2 (Figure S23B). Interestingly, the ^{1}H NMR spectrum of this solution indicated reproduction of the capsule structure **C5′**. These results suggest that the capsule **C5′** is kinetically as well as thermodynamically stable in solution, but the 2D coordination-bonded porous network sheet **S5′** is thermodynamically stable in the crystalline state (Figure 11). This structural interconversion between **C5′** in solution and **S5′** in the crystalline state occurs through reversible Pd–Npy coordination bonds and probably because the crystal packing force of **S5′** is thermodynamically more favorable than that of **C5′**.

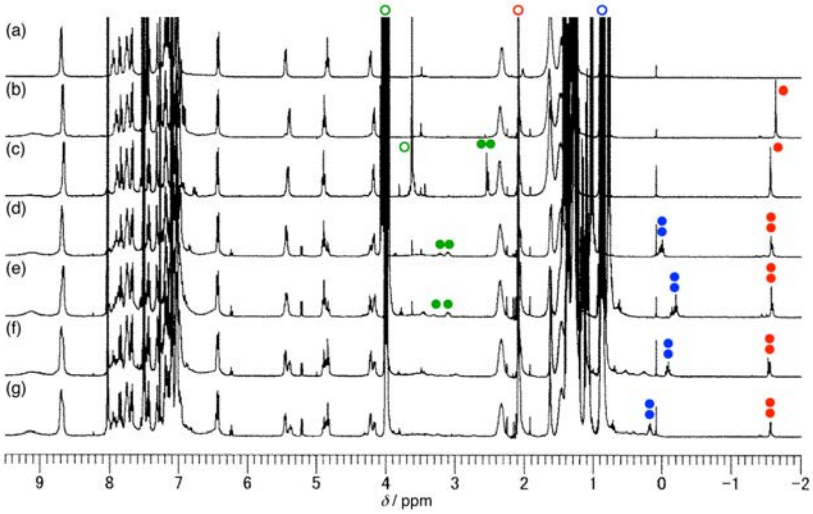

Figure 13. Association behavior of chiral capsule **C5** with guest **G2** or **G5**~**G9** monitored by ^{1}H NMR (400 MHz, $CDCl_3$, 298 K): (a) **C5** alone (1 mM), (b) **G2@C5** ([**C5**] = 1 mM + [**G2**] = 10 mM), (c) **G5@C5** ([**C5**] = 1 mM + [**G5**] = 10 mM), (d) **G6@C5** ([**C5**] = 1 mM + [**G6**] = 10 mM), (e) **G7@C5** ([**C5**] = 1 mM + [**G7**] = 18 mM), (f) **G8@C5** ([**C5**] = 1 mM + [**G8**] = 10 mM), and (g) **G9@C5** ([**C5**] = 1 mM + [**G9**] = 18 mM). The representative signals of encapsulated and free guests are marked with solid and open circles, respectively. The signals of the propynyl-CH_3 groups, the terminal CH_3 groups of the $CO_2(CH_2)_nCH_3$ groups (**G6**~**G9**; n = 1~4), and the CO_2CH_3 (**G5**; n = 0) or the basal CH_2 groups of the $CO_2(CH_2)_nCH_3$ groups (**G6**~**G9**; n = 1~4) are marked with red, blue, and green circles, respectively. See also Scheme 5.

Chiral induction of prochiral biphenyl guest upon encapsulation in chiral capsule C5

Chiral induction of a prochiral guest upon encapsulation in a chiral capsule would be important for supramolecular nanospace chemistry[21] because such an encapsulation design is related to asymmetric capsular catalysts[22] and to the emergence of novel stereoisomerisms.[23] Chiral capsule $\{\mathbf{1}_2\cdot[Pd((R)\text{-BINAP})]_4\}^{8+}\cdot(TfO^-)_8$ (**C5**) encapsulates one guest molecule such as 4,4′-bis(1-propynyl)biphenyl (**G2**) and prochiral 2,2′-bis(alkoxycarbonyl)-4,4′-bis(1-propynyl)biphenyls (**G5**~**G9**) (Scheme 5). We found that chiral capsule **C5** induces supramolecular chirality with respect to prochiral **G5**~**G9** upon encapsulation. Guest-encapsulation behaviors of **C5** were investigated by ^{1}H NMR spectroscopy in $CDCl_3$ at 298 K (Figure 13).

The K_a value of **C5** with **G2** was estimated to be 1.64×10^3 M^{-1}, and the $\Delta\delta$ value for the protons of the 1-propynyl groups of **G2** was –3.73 ppm (Figures 13b and S24). Compared with $K_a = 9.53 \times 10^3$ M^{-1} and $\Delta\delta$ = –3.52 ppm for **G2@C1** (Figures 2d and S8), this result indicates that the cavity length of **C5** composed of **1** with Pd((*R*)-BINAP) is somewhat shorter than that of **C1** composed of **1** with Pd(dppp).

The K_a value of **C5** with 2,2′-bis(methoxycarbonyl)-4,4′-bis(1-propynyl)biphenyl (**G5**) (R′ = CH_3; n = 0) was estimated to be 1.32×10^3 M^{-1}, and the $\Delta\delta$ value for the 1-propynyl group of **G5** was –3.65 ppm (Figures 13c and S25). Compared with $K_a = 3.32 \times 10^3$ M^{-1} and $\Delta\delta$ = –3.53 ppm for **G5@C1** (Figure S26), this result also supports the conclusion that the cavity length of **C5** is somewhat shorter than that of **C1**. The $\Delta\delta$ values for the CO_2CH_3 groups of **G5** were –1.08 and –1.11 ppm for **G5@C5** and –1.10 ppm for **G5@C1**, the values of which were much smaller than the $\Delta\delta$ values for the 1-propynyl groups of **G5@C5** and **G5@C1**. These results indicate that the 1-propynyl groups at the 4,4′-positions of **G5** are oriented toward both aromatic cavity ends of **C5** and **C1**, and the CO_2CH_3 groups at the 2,2′-positions of **G5** are directed to two of the four equatorial windows of **C5** and **C1** (Scheme 5).

The ^{1}H NMR signal of the CO_2CH_3 group of **G5** encapsulated in chiral capsule **C5** notably appeared as two sets of singlets at 2.54 and 2.51 ppm ($\Delta\delta$ = –1.08 and –1.11 ppm) (Figures 13c and S25f), whereas the signal of the CO_2CH_3 group of **G5** encapsulated in achiral capsule **C1** appeared as one singlet at 2.52 ppm ($\Delta\delta$ = –1.10 ppm) (Figure S26f). This result indicates that chiral induction of prochiral **G5** occurred upon encapsulation in the chiral capsule **C5** through asymmetric suppression of rotation around the axis of the prochiral biphenyl moiety in **G5**; that is, diastereomeric complexes (*R*)-**G5@C5** and (*S*)-**G5@C5** were produced on the NMR time-scale (Scheme 5).[21] The diastereomeric excess (*d.e.*) resulting from diastereomeric encapsulation selectivity of **G5@C5** based on the ^{1}H NMR signal integration ratios of the two CO_2CH_3 signals was estimated to be 20%. At this stage, it is not easy to establish which enantiomer of (*R*)- or (*S*)-**G5** is more favorably encapsulated in chiral capsule **C5**, and further studies are required in this regard.

The K_a values, the *d.e.* values, and the $\Delta\delta$ values of the propynyl CH_3 groups and the terminal CH_3 groups of the $CO_2(CH_2)_nCH_3$ groups of guests for the association of **C5** with **G5**~**G9** (alkyl chains R′ = $(CH_2)_nCH_3$; n = 0~4) in $CDCl_3$ at 298 K are summarized in Table 1.

The K_a value of **C5** with 2,2′-bis(ethoxycarbonyl)-4,4′-bis(1-propynyl)biphenyl (**G6**) (n = 1) was estimated to be 257 M^{-1} (Figures 13d and S27). For **G6@C5**, the ^{1}H NMR signals of the 1-propynyl group and the $CO_2CH_2CH_3$ group as well as the $CO_2CH_2CH_3$ group split into two sets of signals at –1.57 and –1.59 ppm ($\Delta\delta$ = –3.66 and –3.68 ppm), 0.031 and –0.008 ppm ($\Delta\delta$ = –0.993 and –1.032 ppm), and 3.22 and 3.10 ppm ($\Delta\delta$ = –0.83 and –0.95 ppm), respectively (Figures 13d and S27e). The diastereomeric encapsulation selectivity of **G6@C5** was estimated to be 22%.

Table 1. The K_a values, the *d.e.* values, and the $\Delta\delta$ values of the propynyl CH_3 groups (A) and the terminal CH_3 groups (B) of the $CO_2(CH_2)_nCH_3$ groups of guests for the association of **C5** with **G5**~**G9** (alkyl chains R′ = $(CH_2)_nCH_3$; n = 0~4) in $CDCl_3$ at 298 K.

G@C5	K_a (M^{-1})	*d.e.* (%)	A, $\Delta\delta$ (ppm)	B, $\Delta\delta$ (ppm)
G5 (n = 0)	1,320	20	–3.65	–1.08, –1.11
G6 (n = 1)	257	22	–3.66, –3.68	–0.99, –1.03
G7 (n = 2)	143	40	–3.66, –3.69	–0.92, –0.97
G8 (n = 3)	58	13	–3.62, –3.65	–0.92, –0.94
G9 (n = 4)	37	<3	–3.65, –3.66	–0.68, –0.70

The K_a value of **C5** with 2,2′-bis(n-propoxycarbonyl)-4,4′-bis(1-propynyl)biphenyl (**G7**) (n = 2) was estimated to be 143 M^{-1} (Figures 13e and S28). The ^{1}H NMR signals of the 1-propynyl group and the $CO_2(CH_2)_2CH_3$ group split into two sets of signals at –1.58 and –1.60 ppm ($\Delta\delta$ = –3.66 and –3.69 ppm) and –0.147 and –0.200 ppm ($\Delta\delta$ = –0.918 and –0.970 ppm), respectively (Figures 13e and S28h). The diastereomeric encapsulation selectivity of **G7@C5** was estimated to be 40%. The ^{1}H NMR spectra for the association of **C5** with **G8** (n = 3) or **G9** (n = 4) are shown in Figures 13f and S29e for **G8@C5** and Figures 13g and S30h for **G9@C5**.

As shown in Table 1, the K_a values and the $\Delta\delta$ values of the terminal CH_3 groups of the $CO_2(CH_2)_nCH_3$ groups of guests for the association of **C5** with **G5**~**G9** (n = 0~4) sequentially decreased with the elongation of the alkyl chains of the $CO_2(CH_2)_nCH_3$ groups of **G5**~**G9**. These results suggest that the alkyl chains of the $CO_2(CH_2)_nCH_3$ groups of **G5**~**G9** encapsulated in **C5** cannot protrude from the equatorial windows of **C5**, and buckling (bending) of longer alkyl chains of the $CO_2(CH_2)_nCH_3$ groups occurs inside the cavity of **C5**,[29] probably because the equatorial windows of **C5** are too small or narrow to allow protrusion of longer alkyl chains of the $CO_2(CH_2)_nCH_3$ groups of guests. If the equatorial windows of **C5** are large enough to allow protrusion of longer alkyl chains of the $CO_2(CH_2)_nCH_3$ groups of guests, the decrease of the K_a values would be prevented[16d,30,31] and increase of the *d.e.* values might be expected with the elongation of the alkyl chains of the $CO_2(CH_2)_nCH_3$ groups of **G5**~**G9**.[21] This is not the case for the association of **C5** with **G5**~**G9**. The diastereomeric encapsulation selectivity for the association of **C5** with **G5**~**G9** showed maximum value (*d.e.* = 40%) for **G7** (n = 2) among them.

Conclusion

We have demonstrated that the components of a 2:4 mixture of tetrakis[4-(4-pyridyl)phenyl]cavitand (**1**) or tetrakis[4-(4-pyridyl)phenylethynyl]cavitand (**2**) and Pd(dppp)$(OTf)_2$ self-assemble into homocapsules $\{\mathbf{1}_2\cdot[Pd(dppp)]_4\}^{8+}\cdot(TfO^-)_8$ (**C1**) and $\{\mathbf{2}_2\cdot[Pd(dppp)]_4\}^{8+}\cdot(TfO^-)_8$ (**C2**), respectively, through Pd–Npy coordination bonds. We comprehensively investigated cavitand-based Pd–Npy coordination capsules to disclose their properties upon guest encapsulation.

Self-sorting in the self-assembled capsule formation through selection between homomeric assembly and heteromeric assembly is an interesting topic in supramolecular chemistry. We have demonstrated that selective formation of homo- or heterocapsule is controllable by guest-induced encapsulation. A 1:1:4 mixture of **1**, **2**, and Pd(dppp)$(OTf)_2$ in the absence of guest produced a mixture of homocapsules **C1**, **C2**, and a heterocapsule $\{\mathbf{1}\cdot\mathbf{2}\cdot[Pd(dppp)]_4\}^{8+}\cdot(TfO^-)_8$ (**C3**) in a 1:1:0.98 mole ratio under thermodynamic control. Upon addition of excess bis(4-acetoxyphenyl)acetylene (**G1**), the mixture of **C1**, **C2**, and **C3** described above was thermodynamically shifted to **G1@C1/C1/C2/C3** = 45:5:50:0. In contrast, upon addition of excess 4,4′′-diacetoxy-*p*-terphenyl (**G3**), the above-mentioned mixture of **C1**, **C2**, and **C3** was thermodynamically shifted to **C1/C2/C3/G3@C3** = 13:13:11:63, wherein a thermodynamic equilibration was shifted most favorably toward formation of **G3@C3** through **G3**-induced stabilization of **C3** by encapsulation.

Applications of Pd–Npy coordination capsules with the use of **1** have been investigated. We have demonstrated that capsule **C1** serves as a guard nanocontainer for *trans*-4,4′-diacetoxyazobenzene (*trans*-**G4**) to protect against the *trans*-to-*cis* photoisomerization of *trans*-**G4** by encapsulation in **C1**, wherein confined space of *trans*-**G4@C1** interferes with geometrical change in the transition state of *trans*-to-*cis* photoisomerization of *trans*-**G4**. A chiral capsule $\{\mathbf{1}_2\cdot[Pd((R)\text{-BINAP})]_4\}^{8+}\cdot(TfO^-)_8$ (**C5**: R = $(CH_2)_{10}CH_3$) made up of the components of a 2:4 mixture of **1** and Pd((*R*)-BINAP)$(OTf)_2$ was also constructed. The unique structural interconversion between capsule **C5′** (R = $CH_2CH(CH_3)_2$) in solution and an infinite two-dimensional Pd–Npy coordination-bonded porous network sheet structure $[\{\mathbf{1'}\cdot[Pd((R)\text{-BINAP})]_2\}^{4+}\cdot(TfO^-)_4]_n$ (**S5′**) in the crystalline state was observed. We found that chiral capsule **C5** induces supramolecular chirality with respect to prochiral biphenyl guests 2,2′-bis(alkoxycarbonyl)-4,4′-bis(1-propynyl)biphenyls (**G5**~**G9**: alkyl chains R′ = $(CH_2)_nCH_3$; n = 0~4) by diastereomeric encapsulation through the asymmetric suppression of rotation around the axis of the prochiral biphenyl moiety upon encapsulation in **C5**. The diastereomeric encapsulation selectivity for the association of **C5** with **G5**~**G9** showed maximum value (*d.e.* = 40%) for **G7** (n = 2) among them.

Further studies of chiral capsules composed of cavitand **1** and various Pd-chiral ligands are expected to endow this type of capsule with characteristics that should help in the development of functional materials, which would constitute an important advance in supramolecular nanospace chemistry.

Experimental Section

The detailed synthesis and characterization of all the compounds are described in the Supporting Information. CCDC 1998707 contains the supplementary crystallographic data for this paper. This data is provided free of charge by The Cambridge Crystallographic Data Centre and Fachinformationszentrum Karlsruhe Access Structures service.

Acknowledgement

This work was supported in part by a JSPS KAKENHI Grant Number JP 17H03021.

Keywords: cage compounds • cavitands • host-guest systems • self-assembly • supramolecular chemistry

[1] a) J. Rebek, Jr., *Angew. Chem. Int. Ed.* **2005**, *44*, 2068-2078; *Angew. Chem.* **2005**, *117*, 2104-2115; b) M. Yoshizawa, J. K. Klosterman, M. Fujita, *Angew. Chem. Int. Ed.* **2009**, *48*, 3418-3438; *Angew. Chem.* **2009**, *121*, 3470-3490; c) K. Kobayashi, M. Yamanaka, *Chem. Soc. Rev.* **2015**, *44*, 449-466; d) H. Sepehrpour, W. Fu, Y. Sun, P. J. Stang, *J. Am. Chem. Soc.* **2019**, *141*, 14005-14020.

[2] a) C. J. Brown, F. D. Toste, R. G. Bergman, K. N. Raymond, *Chem. Rev.* **2015**, *115*, 3012-3035; b) A. J. McConnell, C. S. Wood, P. P. Neelakandan, J. R. Nitschke, *Chem. Rev.* **2015**, *115*, 7729-7793; c) L. You, D. Zha, E. V. Anslyn, *Chem. Rev.* **2015**, *115*, 7840-7892.

[3] For $Pd(Py)_2L_2$-based capsules, see: a) M. Fujita, M. Tominaga, A. Hori, B. Therrien, *Acc. Chem. Res.* **2005**, *38*, 371-380; b) R. Chakrabarty, P. S. Mukherjee, P. J. Stang, *Chem. Rev.* **2011**, *111*, 6810-6918.

[4] For $Pd(Py)_4$-based capsules, see: a) M. Tominaga, K. Suzuki, M. Kawano, T. Kusukawa, T. Ozeki, S. Sakamoto, K. Yamaguchi, M. Fujita, *Angew. Chem. Int. Ed.* **2004**, *43*, 5621-5625; *Angew. Chem.* **2004**, *116*, 5739-5743; b) S. Hiraoka, Y. Yamauchi, R. Arakane, M. Shionoya, *J. Am. Chem. Soc.* **2009**, *131*, 11646-11647; c) N. Kishi, Z. Li, K. Yoza, M. Akita, M. Yoshizawa, *J. Am. Chem. Soc.* **2011**, *133*, 11438-11441; d) K. Harris, D. Fujita, M. Fujita, *Chem. Commun.* **2013**, *49*, 6703-6712; e) M. Han, D. M. Engelhard, G. H. Clever, *Chem. Soc. Rev.* **2014**, *43*, 1848-1860; f) D. Fujita, Y. Ueda, S. Sato, N. Mizuno, T. Kumasaka, M. Fujita, *Nature* **2016**, *540*, 563-566; g) D. P. August, G. S. Nichol, P. J. Lusby, *Angew. Chem. Int. Ed.* **2016**, *55*, 15022-15026; *Angew. Chem.* **2016**, *128*, 15246-15250; h) L. Escobar, E. C. Escudero-Adán, P. Ballester, *Angew. Chem. Int. Ed.* **2019**, *58*, 16105-16109; *Angew. Chem.* **2019**, *131*, 16251-16255.

[5] For metal-coordination assisted tetrahedron- or octahedron-shaped capsules, see: a) D. L. Caulder, K. N. Raymond, *Acc. Chem. Res.* **1999**, *32*, 975-982; b) S. Hiraoka, K. Harano, M. Shiro, Y. Ozawa, N. Yasuda, K. Toriumi, M. Shionoya, *Angew. Chem. Int. Ed.* **2006**, *45*, 6488-6491; *Angew. Chem.* **2006**, *118*, 6638-6641; c) A. M. Castilla, W. J. Ramsay, J. R. Nitschke, *Acc. Chem. Res.* **2014**, *47*, 2063-2073.

[6] For cavitand-based coordination capsules, see: a) F. Fochi, P. Jacopozzi, E. Wegelius, K. Rissanen, P. Cozzini, E. Marastoni, E. Fisicaro, P. Manini, R. Fokkens, E. Dalcanale, *J. Am. Chem. Soc.* **2001**, *123*, 7539-7552; b) R. Pinalli, V. Cristini, V. Sottili, S. Geremia, M. Campagnolo, A. Caneschi, E. Dalcanale, *J. Am. Chem. Soc.* **2004**, *126*, 6516-6517; c) K. Kobayashi, Y. Yamada, M. Yamanaka, Y. Sei, K. Yamaguchi, *J. Am. Chem. Soc.* **2004**, *126*, 13896-13897; d) M. Yamanaka, Y. Yamada, Y.; Sei, K. Yamaguchi, K. Kobayashi, *J. Am. Chem. Soc.* **2006**, *128*, 1531-1539; e) T. Haino, M. Kobayashi, Y. Fukazawa, *Chem. Eur. J.* **2006**, *12*, 3310-3319; f) Y. Tsunoda, K. Fukuta, T. Imamura, R. Sekiya, T. Furuyama, N. Kobayashi, T. Haino, *Angew. Chem. Int. Ed.* **2014**, *53*, 7243-7247; *Angew. Chem.* **2014**, *126*, 7371-7375; g) T. Imamura, T. Maehara, R. Sekiya, T. Haino, *Chem. Eur. J.* **2016**, *22*, 3250-3254; h) L. He, S.-C. Wang, L.-T. Lin, J.-Y. Cai, L. Li, T.-H. Tu, Y.-T. Chan, *J. Am. Chem. Soc.* **2020**, *142*, 7134-7144.

[7] A. Wu, L. Isaacs, *J. Am. Chem. Soc.* **2003**, *125*, 4831-4835.

[8] For self-sorting for hydrogen-bonded self-assembled capsules, see: a) D. Ajami, M. P. Schramm, A. Volonterio, J. Rebek, Jr., *Angew. Chem. Int. Ed.* **2007**, *46*, 242-244; *Angew. Chem.* **2007**, *119*, 246-248; b) D. Ajami, J.-L. Hou, T. J. Dale, E. Barrett, J. Rebek, Jr., *Proc. Natl. Acad. Sci. U.S.A.* **2009**, *106*, 10430-10434; c) H. Jedrzejewska, M. Wierzbicki, P. Cmoch, K. Rissanen, A. Szumna, *Angew. Chem. Int. Ed.* **2014**, *53*, 13760-13764; *Angew. Chem.* **2014**, *126*, 13980-13984.

[9] For self-sorting for self-assembled capsules based on metal-coordination bonds, see: a) S. Hiraoka, Y. Kubota, M. Fujita, *Chem. Commun.* **2000**, 1509-1510; b) C. Gütz, R. Hovorka, G. Schnakenburg, A. Lützen, *Chem. Eur. J.* **2013**, *19*, 10890-10894; c) N. Sinha, T. T. Y. Tan, E. Peris, F. E. Hahn, *Angew. Chem. Int. Ed.* **2017**, *56*, 7393-7397; *Angew. Chem.* **2017**, *129*, 7499-7503; d) Y.-S. Wang, T. Feng, Y.-Y. Wang, F. E. Hahn, Y.-F. Han, *Angew. Chem. Int. Ed.* **2018**, *57*, 15767-15771; *Angew. Chem.* **2018**, *130*, 15993-15997; e) T. Tateishi, T. Kojima, S. Hiraoka, *Commun. Chem.* **2018**, *1*, 20; f) S. Kai, T. Kojima, F. L. Thorp-Greenwood, M. J. Hardie, S. Hiraoka, *Chem. Sci.* **2018**, *9*, 4104-4108; g) T. R. Schulte, J. J. Holstein, G. H. Clever, *Angew. Chem. Int. Ed.* **2019**, *58*, 5562-5566; *Angew. Chem.* **2019**, *131*, 5618-5622; h) F. J.; Rizzuto, J. P. Carpenter, J. R. Nitschke, *J. Am. Chem. Soc.* **2019**, *141*, 9087-9095.; i) D. Bardhan, D. K. Chand, *Chem. Eur. J.* **2019**, *25*, 12241-12269; j) A. Kumar, P. S. Mukherjee, *Chem. Eur. J.* **2020**, *26*, 4842-4849.

[10] For self-sorting for self-assembled capsules based on dynamic imine bonds, see: a) K. Acharyya, S. Mukherjee, P. S. Mukherjee, *J. Am. Chem. Soc.* **2013**, *135*, 554-557; b) D. Beaudoin, F. Rominger, M. Mastalerz, *Angew. Chem. Int. Ed.* **2017**, *56*, 1244-1248; *Angew. Chem.* **2017**, *129*, 1264-1268; c) M. Kolodziejski, A. R. Stefankiewicz, J.-M. Lehn, *Chem. Sci.* **2019**, *10*, 1836-1843; d) R. L. Greenaway, V. Santolini, A. Pulido, M. A. Little, B. M. Alston, M. E. Briggs, G. M. Day, A. I. Cooper, K. E. Jelfs, *Angew. Chem. Int. Ed.* **2019**, *58*, 16275-16281; *Angew. Chem.* **2019**, *131*, 16421-16427.

[11] For chiral self-sorting, see: a) H. Jedrzejewska, A. Szumna, *Chem. Rev.* **2017**, *117*, 4863-4899; b) Ref. [9b]; c) Ref. [9e]; d) Ref. [9f]; e) Ref. [9g]; f) Ref. [10b].

[12] For self-sorting for self-assembled capsule based on van der Waals and hydrophobic interactions, see: Y.-Y. Zhan, T. Kojima, K. Ishii, S. Takahashi, Y. Haketa, H. Maeda, S. Uchiyama, S. Hiraoka, *Nature Commun.* **2019**, *10*, 1440.

[13] For stabilization of very unstable chemical species in covalently bound capsules, see: R. Warmuth, J. Yoon, *Acc. Chem. Res.* **2001**, *34*, 95-105.

[14] For stabilization of reaction intermediates in self-assembled capsules, see: a) M. Yoshizawa, T. Kusukawa, M. Kawano, T. Ohhara, I. Tanaka, K. Kurihara, N. Niimura, M. Fujita, *J. Am. Chem. Soc.* **2005**, *127*, 2798-2799; b) D. Fiedler, R. G. Bergman, K. N. Raymond, *Angew. Chem. Int. Ed.* **2006**, *45*, 745-748; *Angew. Chem.* **2006**, *118*, 759-762; c) T. Iwasawa, E. Mann, J. Rebek, Jr., *J. Am. Chem. Soc.* **2006**, *128*, 9308-9309; d) V. M. Dong, D. Fiedler, B. Carl, R. G. Bergman, K. N. Raymond, *J. Am. Chem. Soc.* **2006**, *128*, 14464-14465.

[15] For safe storage of hazardous chemicals in self-assembled capsules, see: a) P. Mal, B. Breiner, K. Rissanen, J. R. Nitschke, *Science* **2009**, *324*, 1697-1699; b) M. Yamashina, Y. Sei, M. Akita, M. Yoshizawa, *Nature Commun.* **2014**, *5*, 4662.

[16] For enhancement of photostability and control over photophysical properties of organic dyes by encapsulation in self-assembled capsules, see: a) L. S. Kaanumalle, C. L. D. Gibb, B. C. Gibb, V. Ramamurthy, *J. Am. Chem. Soc.* **2005**, *127*, 3674-3675; b) M. R. Ams, D. Ajami, S. L. Craig, J.-S. Yang, J. Rebek, Jr., *J. Am. Chem. Soc.* **2009**, *131*, 13190-13191; c) N. Nishimura, K. Kobayashi, *J. Org. Chem.* **2010**, *75*, 6079-6085; d) Y. Hirumi, K. Tamaki, T. Namikawa, K. Kamada, M. Mitsui, K. Suzuki, K. Kobayashi, *Chem. Asian J.* **2014**, *9*, 1282-1290; e) A. M. Raj, G. Sharma, R. Prabhakar, V. Ramamurthy, *Org. Lett.* **2019**, *21*, 5243-5247.

[17] O. B. Berryman, H. Dube, J. Rebek, Jr., *Isr. J. Chem.* **2011**, *51*, 700-709.

[18] For reviews of self-assembled chiral capsules, see: a) M. A. Mateos-Timoneda, M. Crego-Calama, D. N. Reinhoudt, *Chem. Soc. Rev.* **2004**, *33*, 363-372; b) A. Scarso, J. Rebek, Jr., *Top. Curr. Chem.* **2006**, *265*, 1-46; c) G. Seeber, B. E. F. Tiedemann, K. N. Raymond, *Top. Curr. Chem.* **2006**, *265*, 147-183.

[19] For chiral molecular recognition of racemic guests by using self-assembled chiral capsules, see: a) R. K. Castellano, B. H. Kim, J. Rebek, Jr., *J. Am. Chem. Soc.* **1997**, *119*, 12671-12672; b) R. K. Castellano, C. Nuckolls, J. Rebek, Jr., *J. Am. Chem. Soc.* **1999**, *121*, 11156-11163; c) J. M. Rivera, T. Martin, J. Rebek, Jr., *J. Am. Chem. Soc.* **2001**, *123*, 5213-5220; d) D. Fiedler, D. H. Leung, R. G. Bergman, K. N. Raymond, *J. Am. Chem. Soc.* **2004**, *126*, 3674-3675; e) C. J. Hastings, M. D. Pluth, S. M. Biros, R. G. Bergman, K. N. Raymond, *Tetrahedron* **2008**, *64*, 8362-8367; f) A. Szumna, *Chem. Eur. J.* **2009**, *15*, 12381-12388; g) A. U. Malik, F. Gan, C. Shen, N. Yu, R. Wang, J. Crassous, M. Shu, H. Qiu, *J. Am. Chem. Soc.* **2018**, *140*, 2769-2772.

[20] A. Ikeda, H. Udzu, Z. Zhong, S. Shinkai, S. Sakamoto, K. Yamaguchi, *J. Am. Chem. Soc.* **2001**, *123*, 3872-3877.

[21] K. Tamaki, A. Ishigami, Y. Tanaka, M. Yamanaka, K. Kobayashi, *Chem. Eur. J.* **2015**, *21*, 13714-13722.

[22] a) Y. Nishioka, T. Yamaguchi, M. Kawano, M. Fujita, *J. Am. Chem. Soc.* **2008**, *130*, 8160-8161; b) C. J. Brown, R. G. Bergman, K. N. Raymond, *J. Am. Chem. Soc.* **2009**, *131*, 17530-17531; c) C. Tan, D. Chu, X. Tang, Y. Liu, W. Xuan, Y. Cui, *Chem. Eur. J.* **2019**, *25*, 662-672; d) Y. Fang, J. A. Powell, E. Li, Q. Wang, Z. Perry, A. Kirchon, X. Yang, Z. Xiao, C. Zhu, L. Zhang, F. Huang, H.-C. Zhou, *Chem. Soc. Rev.* **2019**, *48*, 4707-4730.

[23] a) T. Amaya, J. Rebek, Jr., *J. Am. Chem. Soc.* **2004**, *126*, 6216-6217; b) M. P. Schramm, J. Rebek, Jr., *New J. Chem.* **2008**, *32*, 794-796.

[24] M. Nakamura, K. Kishimoto, Y. Kobori, T. Abe, K. Yoza, K. Kobayashi, *J. Am. Chem. Soc.* **2016**, *138*, 12564-12577.

[25] Capsule **C2** did not encapsulate bis(4-acetoxyphenyl)butadiyne (molecular length (L) = 19.35 Å), 4-acetoxy-(4′-acetoxyphenylethynyl)biphenyl (L = 21.28 Å), and 4,4′′′-diacetoxy-*p*-quaterphenyl (L = 22.88 Å), in addition to **G3** (L = 18.54 Å).

[26] Photoirradiation was conducted with a 300 W Xe lamp through a color filter for 350 nm light.

[27] a) B. Olenyuk, J. A. Whiteford, P. J. Stang, *J. Am. Chem. Soc.* **1996**, *118*, 8221-8230; b) M. Ayabe, K. Yamashita, K. Sada, S. Shinkai, A. Ikeda, S. Sakamoto, K. Yamaguchi, *J. Org. Chem.* **2003**, *68*, 1059-1066.

[28] Tetragonal, space group = *I*4, $a = b$ = 19.7850(7) Å, c = 33.6641(14) Å, $\alpha = \beta = \gamma = 90°$, V = 13177.7(11) Å^3, Z = 8, T = 90 K, GOF on F^2 = 1.102, R_1 = 0.0689 ($I > 2\sigma(I)$), wR_2 = 0.2024 (all data). CCDC deposition number: CCDC 1998707.

[29] M. Yamanaka, A. Shivanyuk, J. Rebek, Jr., *J. Am. Chem. Soc.* **2004**, *126*, 2939-2943.

[30] a) H. Kitagawa, Y. Kobori, M. Yamanaka, K. Yoza, K. Kobayashi, *Proc. Natl. Acad. Sci. U.S.A.* **2009**, *106*, 10444-10448; b) K. Ichihara, H. Kawai, Y. Togari, E. Kikuta, H. Kitagawa, S. Tsuzuki, K. Yoza, M. Yamanaka, K. Kobayashi, *Chem. Eur. J.* **2013**, *19*, 3685-3692.

[31] N. Nishimura, K. Yoza, K. Kobayashi, *J. Am. Chem. Soc.* **2010**, *132*, 777-790.

WILEY-VCH

Entry for the Table of Contents

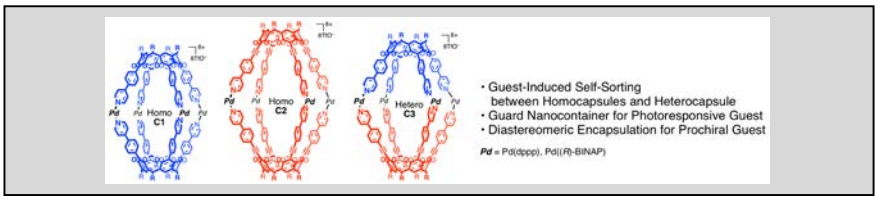

Expanded pyridyl-cavitands form Pd–Npy coordination capsules. These capsules have multiple functions: (1) control of self-sorting on homo- or heterocapsule selection by guest-induced encapsulation, (2) a guard nanocontainer for a photoresponsive guest, and (3) a chiral capsule that induces supramolecular chirality with respect to a prochiral guest.

WILEY-VCH